CrossMark

Effect of Gallium Additions on Reduction, Carburization and Fischer–Tropsch Activity of Iron Catalysts

Charles Beasley[1] · Muthu Kumaran Gnanamani[1] · Hussein H. Hamdeh[2] · Michela Martinelli[1] · Burtron H. Davis[1]

Abstract

Undoped and gallium-doped iron oxide catalysts (100Fe, 100Fe:2Ga, and 100Fe:5Ga) were prepared by following a continuous co-precipitation technique using ammonium hydroxide as precipitant. The catalysts were characterized by BET surface area, X-ray diffraction, H_2-temperature programmed reduction, ^{57}Fe Mössbauer spectroscopy, and temperature programmed decarburization techniques. The addition of gallium affects both reduction as well as carburization of iron oxide. The CO conversion decreases with an increase of gallium content relative to iron. The gallium-doped iron catalyst (100Fe:2Ga) exhibits initially a lower CO conversion after H_2 activation than an undoped iron catalyst; however, the activity of the doped catalyst kept increasing with time. A strong interaction between iron oxide and gallium could explain the suppressed formation of χ-Fe_5C_2 and metallic iron during the carburization and reduction of iron oxide, respectively. The relative percentage of iron in χ-Fe_5C_2 was found to correlate with the initial rates of FT and WGS activity indicating that iron carbide is the main active component for both FT and WGS reactions.

Graphical Abstract
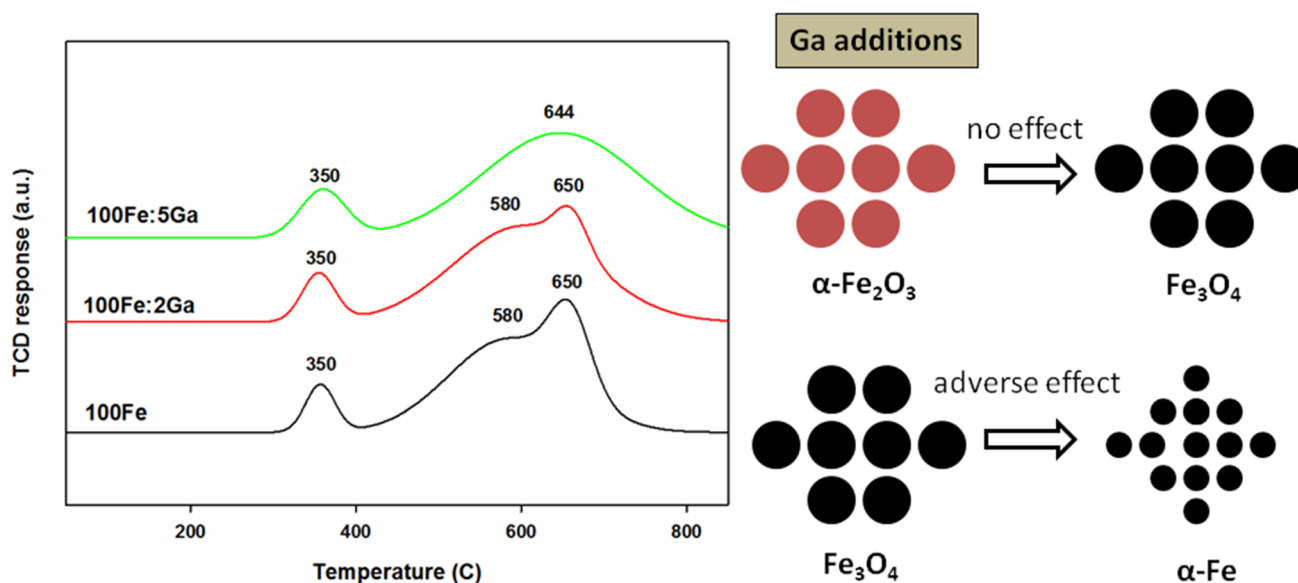
- ✓ Increasing BET surface area
- ✓ Detrimentally affect the reduction of Fe_3O_4 (Fe^{3+}, Fe^{2+}) to Fe
- ✓ Decreasing iron carbide formation
- ✓ Decreasing CO and H_2 conversions

Extended author information available on the last page of the article

1 Introduction

Fischer–Tropsch synthesis (FTS) uses Fe or Co-based catalysts to convert syngas into liquid hydrocarbons which are virtually sulfur and aromatic free transportation fuels [1–3]. Iron-based catalysts are attractive because of their low cost, high FTS activity and intrinsic water–gas shift (WGS) activity that could manage different syngas feed ratios (H_2/CO = 0.5–2.5) [4, 5]. Several factors influence the activity and selectivity of FTS iron catalysts. Often, silica oxide (SiO_2) [6–10] is added as a binder since it helps to stabilize and add more structure to the catalyst, such as helping to increase the surface area, pore density, and amount of pores within the catalyst itself.

Jothimurugesan et al. [6] found that addition of 12 wt% silica to 100Fe/5Cu/2K produces a higher attrition resistance. Also, silica may suppress the reduction of iron oxides and decrease the activity of the catalysts [8–10]. Bukur et al. [8] claimed that the addition of silica and alumina decreased the hydrogenation and WGS activity for the doubly promoted iron catalysts. Jin et al. [9], using electron energy loss spectroscopy (EELS), found that after CO activation the iron phase segregates into iron carbide, leaving some unreduced iron oxide in an amorphous state coexisting with the silica. Dlamini et al. [10] found that silica added either before or after precipitation hindered the reduction and carburization of the doubly promoted (Cu and K) iron catalysts. However, Sirimanothan et al. [11] found the opposite effect for a catalyst series that did not contain Cu.

Although studies such as the effect of silica on iron FTS reaction are often found in the literature, similar investigations using aluminum oxide or gallium oxide for iron Fischer–Tropsch synthesis are not as numerous. In the present study, gallium was added to iron during precipitation from iron nitrate solution at different Ga to Fe ratios (100Fe, 100Fe:2Ga, and 100Fe:5Ga). The influence of addition of Ga on the reduction and carburization of iron oxide was followed using BET surface area, XRD, H_2-TPR, ^{57}Fe Mössbauer spectroscopy, and temperature programmed decarburization techniques. The FTS activity and product selectivity were compared to the active phases of iron.

2 Experimental

2.1 Catalyst Preparation

The precipitated iron catalyst was prepared by using a ferric nitrate solution obtained by dissolving iron (III) nitrate nonahydrate (1.17 M) in deionized water. A controlled flow of the iron nitrate was added to a precipitation vessel together with a stream of ammonium hydroxide (14.8 M) that was added at a rate to maintain a pH of 9.0. In the gallium doped iron catalysts, an appropriate amount of gallium nitrate was mixed with the iron (III) nitrate nonahydrate in order to have the following compositions: 100Fe:2Ga and 100Fe:5Ga. The solid precipitate was recovered using a vacuum filter and the filter cake was then washed and filtered three times with deionized water in order to remove excess ammonia. The final material was dried in an oven at 110 °C for 24 h followed by calcination at 450 °C in flowing air for 6 h. Pure γ-Ga_2O_3 was prepared by the thermal decomposition of gallium nitrate at 450 °C.

2.2 Catalyst Characterization

2.2.1 Surface Area and Pore Size Distribution

BET surface area and porosity characteristics of the calcined catalysts were measured using a Micromeritics 3-Flex system. Before performing the test, the temperature was gradually ramped to 160 °C and the sample was evacuated at this temperature for 12 h to approximately 50 mTorr. The BET surface area, single point pore volume, and single point average pore diameter were obtained for each sample. The Barrett–Joyner–Halenda (BJH) method was also used to estimate pore volume and average pore diameter, as well as to provide pore size distribution as a function of pore radius.

2.2.2 X-Ray Diffraction

Powder X-ray diffractograms of iron catalysts in an oxidized form and after carburization/passivation were recorded using a Philips X'Pert diffractometer with monochromatic Cu Kα radiation (λ = 1.5418). XRD scans were taken over the range of 2θ from 5° to 90°. The scanning step was 0.017°, and the scan speed was 0.042 s^{-1}.

2.2.3 ^{57}Fe Mössbauer Absorption Spectroscopy

^{55}Fe Mössbauer spectra were collected in a transmission mode by a standard constant acceleration spectrometer (MS-1200, Ranger Scientific). A radiation source of 50 mCi ^{57}Co in Rh matrix was used and the spectra were obtained using a gas detector. Following activation, each sample was carefully fixed into wax inside a glove box before being transported for analysis. All samples were investigated at low temperature (− 253 °C) using a closed cycle refrigerator, typically over a velocity range of ± 10 mm/s. Structural

analysis of each sample was carried out by least-squares fitting of the Mössbauer spectra to a summation of hyperfine sextets. Details about the least-squares fitting procedures are described elsewhere [12].

2.2.4 Temperature Programmed Reduction and Temperature Programmed Decarburization

Temperature programmed reduction by H_2 was performed for various iron catalysts using an in-house system consisting of a furnace capable of operating at temperatures up to 1200 °C, along with a thermal conductivity detector (TCD, SRI-GC). H_2-TPR was performed using $10\%H_2/Ar$ at a flow rate of 50 cm^3/min and the catalyst sample (0.2 g) was heated from 30 to 850 °C at a ramp rate of 10 °C/min. The same system was used for carrying out temperature programmed decarburization of various carburized iron catalysts. In this case, initially the iron oxide catalyst (0.2 g) was carburized in flowing CO at 270 °C for 24 h. The temperature of the catalyst was decreased to 30 °C while purging with He and the decarburization was performed in flowing H_2:He (1:3) and the temperature were increased to 850 °C at a ramp rate of 10 °C/min. The origin Pro-8 data analysis and graphing software were used for correcting the background.

2.3 Fischer–Tropsch Synthesis

The FTS reactions were carried out using a 1 l continuously stirred tank reactor (CSTR). Typically, 12.0 g of iron catalyst was mixed with 310 g of melted Polywax-3000. The catalyst was activated by flowing either CO or H_2 (24 slph) at 270 °C and atmospheric pressure for 24 h. The reactor pressure was then increased to 175 psig and the feed gas was switched from CO or H_2 to syngas (H_2:CO) at a mole ratio of 1:1 and a constant space velocity at 3.0 slph/g iron oxide. Brook mass flow controllers were used to control the flow rates of H_2 and CO. The conversions of CO and H_2 were obtained by gas chromatography analysis of reactor exit gas stream using a fusion micro GC from Inficon. The reaction products were collected in two traps maintained at different temperatures—a warm trap (100 °C) and a cold trap (5 °C). The products were separated into different fractions (oil and water) for quantification. The organic phase condensed in the warm and cold traps were analyzed using a HP 7890 GC with a DB-5 capillary column, while the aqueous phase was analyzed using an SRI (Torrance, CA) GC-TCD-8610C with a 6′ Poropak-Q stainless steel packed column. A 5673N MSD coupled to the 6890 GC from Agilent was employed for qualitative analysis of various oxygenated compounds. The conversion and selectivity reaction parameters are defined as:

$$Conversion = 100 \times \frac{n_{CO_{in}} - n_{CO_{out}}}{n_{CO_{in}}}$$

$$Selectivity = 100 \times \frac{n_{product_{out}} \times carbon\ number}{n_{CO_{in}} - n_{CO_{out}}}$$

where $n_{CO_{in}}$ and $n_{CO_{out}}$ are the numbers of moles of CO fed and unconverted, respectively. The selectivity is defined as the percentage of moles of CO consumed to form a particular C_n product (hydrocarbon, CO or oxygenate), normalized by the total amount of CO consumed.

The passivation was performed for the activated iron catalysts by purging under a flow of 1% O_2 in He at room temperature (25 °C) for 5 h. The nature of crystalline phases of activated-passivated catalysts were examined using X-ray diffraction technique.

3 Results and Discussion

Figure 1 shows XRD patterns of iron oxide catalysts with and without gallium additions. The pattern was indexed to a hematite phase (JCPDS#86-0550). The addition of gallium broadened the XRD peaks (33 and 35.6, 2θ) corresponding to hematite phase of iron indicating that the crystallite sizes of iron oxide tend to decrease with gallium addition. From XRD data, the average crystallite size can be calculated using the Scherrer equation below [13]:

$$D = K\lambda\ (\beta\ cos\theta)$$

where D is the average size of the crystallites, K is the Scherrer constant (0.9), λ is the wavelength of radiation (1.5418 Å), β is full width at half maximum (FWHM) of diffraction lines and θ corresponds to the peak position. The estimated average crystallite size of 100Fe catalyst was 24.0 nm and for 100Fe:2Ga and 100Fe:5Ga catalysts, 19.3 and 13.6 nm, respectively.
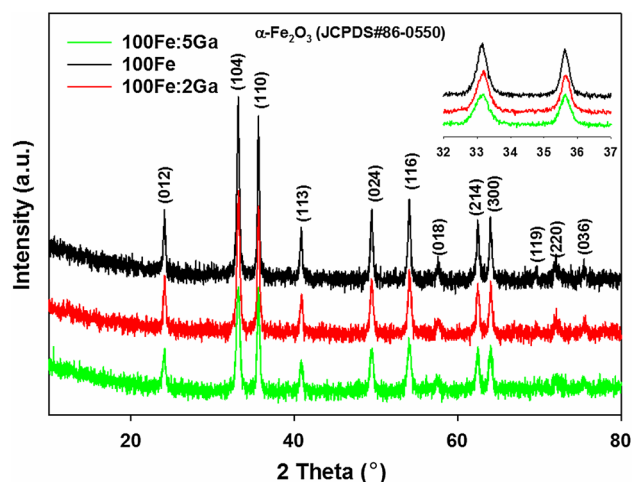

Fig. 1 XRD patterns of iron oxide catalysts, insert shows a magnified portion of 2θ between 32 and 37

BET surface area of the calcined iron oxide was found to be 37.8 m^2/g (Table 1) that increased with increasing gallium to 45.2 and 46.2 m^2/g for the 100Fe:2Ga and 100Fe:5Ga catalysts, respectively. However, both the pore volume and pore diameter of the catalysts did not follow any trend with gallium additions to iron. A slight increase of surface area and a reduction in the crystallite sizes were observed with additions of gallium for calcined iron oxide. This is in line with the effects of addition of silica to iron catalysts, as observed by others [14].

The temperature programmed reduction profiles using hydrogen for various gallium containing iron oxide catalysts are shown in Fig. 2. A typical two-peak reduction pattern was obtained for all gallium-containing iron catalysts; this corresponds to the reduction of Fe^{3+} to Fe^{2+} and the second peak is often ascribed to the successive reduction of the oxides [15]. The undoped and gallium-doped iron catalysts show that the initial reduction peak remained the same and centered at 350 °C. The second peak, centered at 580 °C, shifted toward higher temperatures with gallium additions which shows the strong interaction of iron oxide with gallium. There is a shoulder at 650 °C for 100Fe and 100Fe:2Ga samples but it was not seen promptly in the case of 100Fe:5Ga. At this point, it is not clear whether the shoulder that appears at 650 °C for 100Fe and 100Fe:2Ga could be due to formation of FeO. A detailed in situ XRD or other X-ray absorption studies might answer this question. The reduction of γ-Ga_2O_3 was performed under similar H_2-TPR conditions as done with Fe_2O_3 and other gallium-containing iron catalysts. The γ-Ga_2O_3 sample exhibits (Fig. 2, dotted blue line) a clear reduction peak centered at 390 °C and it could be attributed as due to the surface reduction of gallium oxide [16]. The bulk reduction occurs for gallium oxide at above 700 °C. As such, there was no interference observed from reduction of gallium oxide to the initial reduction of iron oxide. It infers that the gallium additions to iron did not affect Fe^{3+} to Fe^{2+} reduction process. By contrast, the reduction of Fe^{2+} to metallic iron was definitely affected by gallium.
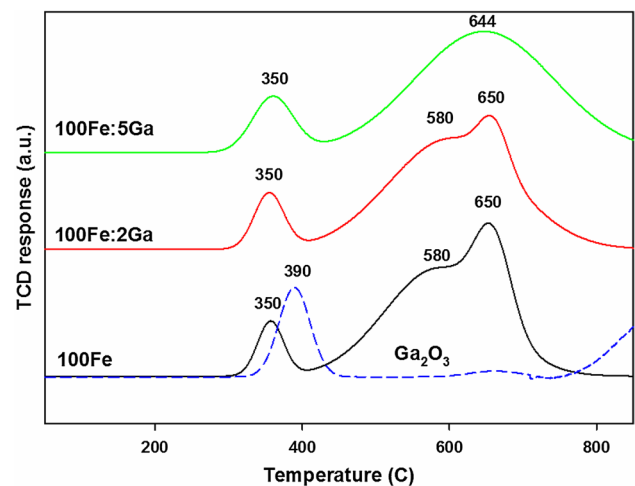

Fig. 2 H_2-TPR profiles of iron oxide catalysts

The quantitative estimation of various iron phases was determined for the activated catalysts using ^{57}Fe Mössbauer absorption spectroscopy performed at -253 °C. The experimentally obtained spectra and the fitting curves for various iron species are shown in Fig. 3. The solid black line indicates the fitted curve, the blue line indicates Hägg carbide, the red line shows magnetite phase and the green line of metallic iron. Figure 3a, b show fitted curves for undoped- and various gallium-doped iron catalysts after CO and H_2 activations, respectively. Hägg carbide (χ-Fe_5C_2) is the major iron phase (88%) present in a freshly CO activated iron catalyst as shown in Table 2 whose percent carbide dropped to 71% for 100Fe:2Ga and 54% for 100Fe:5Ga. Alternatively, the percent of magnetite (Fe_3O_4) increased with an increase of gallium content. A similar trend was obtained with those catalysts reduced under hydrogen; however, the percent of metallic iron was reduced drastically from 60% for 100Fe to 6% for 100Fe:5Ga catalysts. Therefore, both carburization and reduction of iron oxide were impacted by the addition of gallium; however, the extent with which Ga affects both processes are different.

Table 1 BET surface area and pore size distribution

Catalyst description	BET S.A. (m^2/g)	Single point pore volume (cm^3/g)[a]	BJH pore volume (cm^3/g)[b]	Single point average pore diameter (nm)[c]	BJH pore diameter (nm)[d]
100Fe	37.8	0.23	0.223	23.9	20.5
100Fe:2Ga	45.2	0.19	0.192	16.8	13.2
100Fe:5Ga	46.2	0.23	0.233	20.0	16.7

[a]Single-point pore volume obtained from single-point desorption total volume of pores at $P/P_0 = 0.99$

[b]BJH desorption cumulative volume of pores between 1.7 and 300 nm diameter

[c]Desorption average pore diameter by BET

[d]BJH desorption average pore diameter

X-ray diffraction was applied in this study to analyze various iron species present in the activated-passivated iron catalysts. Figure 4 displays the XRD pattern of iron samples after CO or H_2 activation. All three iron catalyst samples (Fig. 4a) exhibit χ-Fe_5C_2 and Fe_3O_4 phases after activation in flowing CO at 270 °C. However, the presence of magnetite phase prevails more in 100Fe:5Ga than 100Fe:2Ga and 100Fe samples. For H_2-reduced iron catalyst samples (Fig. 4b), the intensity corresponding to metallic iron decreases with increasing gallium content. This shows that gallium suppressed the reducibility of iron oxide by involving strong metal-oxide interactions of FeO_x with gallium which could prevent the transition of magnetite to metallic iron under the reduction conditions followed in this work.

Temperature programmed decarburization analysis of a freshly carburized iron catalyst sample is shown in Fig. 5. Hydrogen reacts with iron carbides, carbons and magnetite and forms methane and metallic iron. The hydrogen consumption was followed by TCD. According to Xu and Bartholomew [17], different carbon-containing iron species start reducing at different temperatures. The temperature range between 200 and 400 °C is classified as the low-temperature carbon species, also known as atomic carbon or surface carbide. The middle region between 400 and 600 °C is known as amorphous carbon or β-phase carbons and finally the temperature above 600 °C is classified as carbidic carbon, γ_1, and graphitic carbons, γ_2. The TCD response measured as a function of temperature yields a broad peak at 525 °C for 100Fe catalyst along with a shoulder at 600 °C. The
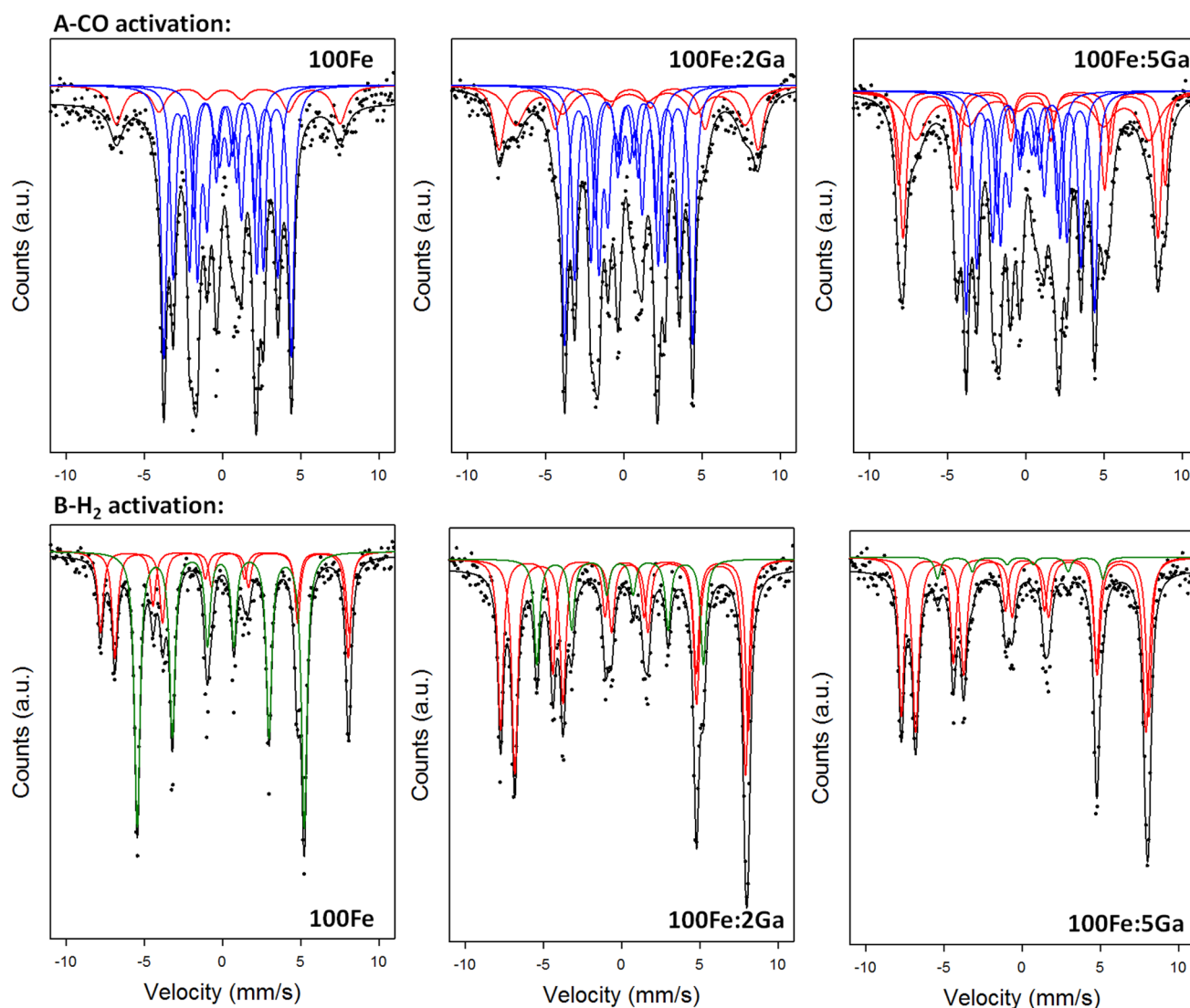

Fig. 3 ^{57}Fe Mössbauer absorption spectrum of activated iron catalysts performed at −253 °C. The fitted curves are shown as a solid line: black, total spectra; red, Fe_3O_4; blue, χ-Fe_5C_2; green, metallic iron

Table 2 Fe phase analysis using ^{57}Fe Mossbauer spectroscopy performed at 253 °C

Catalyst	Iron species (% area)[a]			
	After CO activation		After H$_2$ activation	
	Fe$_3$O$_4$	χ-Fe$_5$C$_2$	Fe$_3$O$_4$	Metallic Fe
100Fe	12	88	40	60
100Fe:2Ga	29	71	79	21
100Fe:5Ga	46	54	94	6

[a]Uncertainty in these numbers varies by 3–5%

primary peak at 525 °C is ascribed to the decarburization of bulk iron carbide. The addition of gallium was found to shift the peak to a higher temperature of 525 °C for 100Fe to 560 °C for 100Fe:2Ga and 570 °C for 100Fe:5Ga. This upward shift in the temperature of decarburization infers that gallium somehow affects the rate of hydrogen consumption by iron carbides. Addition of gallium to iron also moved a shoulder peak to high temperature with its increasing intensity. The temperature programmed reduction profiles using H$_2$, and other characterization studies (XRD, Mössbauer), indicate that magnetite is present in both CO and H$_2$ activated samples. Hence, we assign this shoulder to a reduction of magnetite to metallic iron under these decarburization conditions. This indicates that gallium moderately affects the carburization of iron oxide while it adversely affects their reduction process under an H$_2$ atmosphere.

The FT performances of undoped and gallium-doped iron catalysts after (A) CO and (B) H$_2$ activations are shown in Fig. 6. All iron catalysts activated under CO flow show deactivation. The undoped iron catalyst exhibits the highest CO conversion whose activity decreased from 49 to 40% in 180 h time on-stream (TOS). The CO conversion decreased by 10 and 4% for the 100Fe:2Ga and 100Fe:5Ga catalysts, respectively. On the other hand, the H$_2$ activated iron catalyst exhibited a CO conversion of 30% initially; the conversions dropped to 25% in 50 h TOS but did not show any changes thereafter. The CO conversion of 100Fe:2Ga catalyst was 15% and showed an increasing trend with time. After ~ 170 h TOS the CO, conversion of both the 100Fe and 100Fe:2Ga were similar. The 100Fe:5Ga catalyst also shows an increase of CO conversion with time. This could potentially be due to a phase transformation of iron from metallic to iron carbide under these reaction conditions.

Both 100Fe and 100Fe:5Ga catalyst samples show a very similar methane selectivity which starts at 7% and increases to 11% with time for the CO activated catalysts. However, the 100Fe:2Ga catalyst had a lower methane selectivity (5–7%) than 100Fe and 100Fe:5Ga catalysts. On the other hand, the methane selectivity of the H$_2$ reduced iron catalysts remained relatively constant at about 15%. All the catalysts exhibit a nearly steady trend
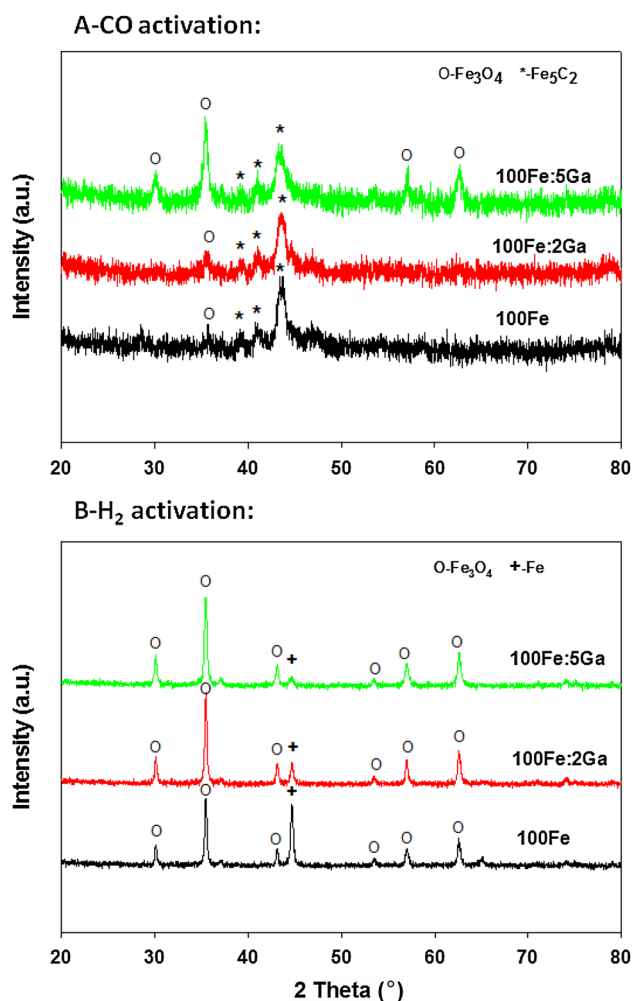

Fig. 4 XRD patterns of freshly activated iron catalysts **a** CO and **b** H$_2$ after passivation in flowing 1% O$_2$/He at 25 °C
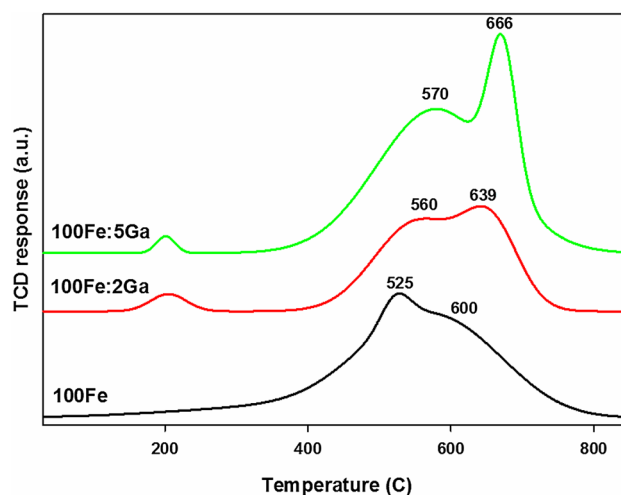

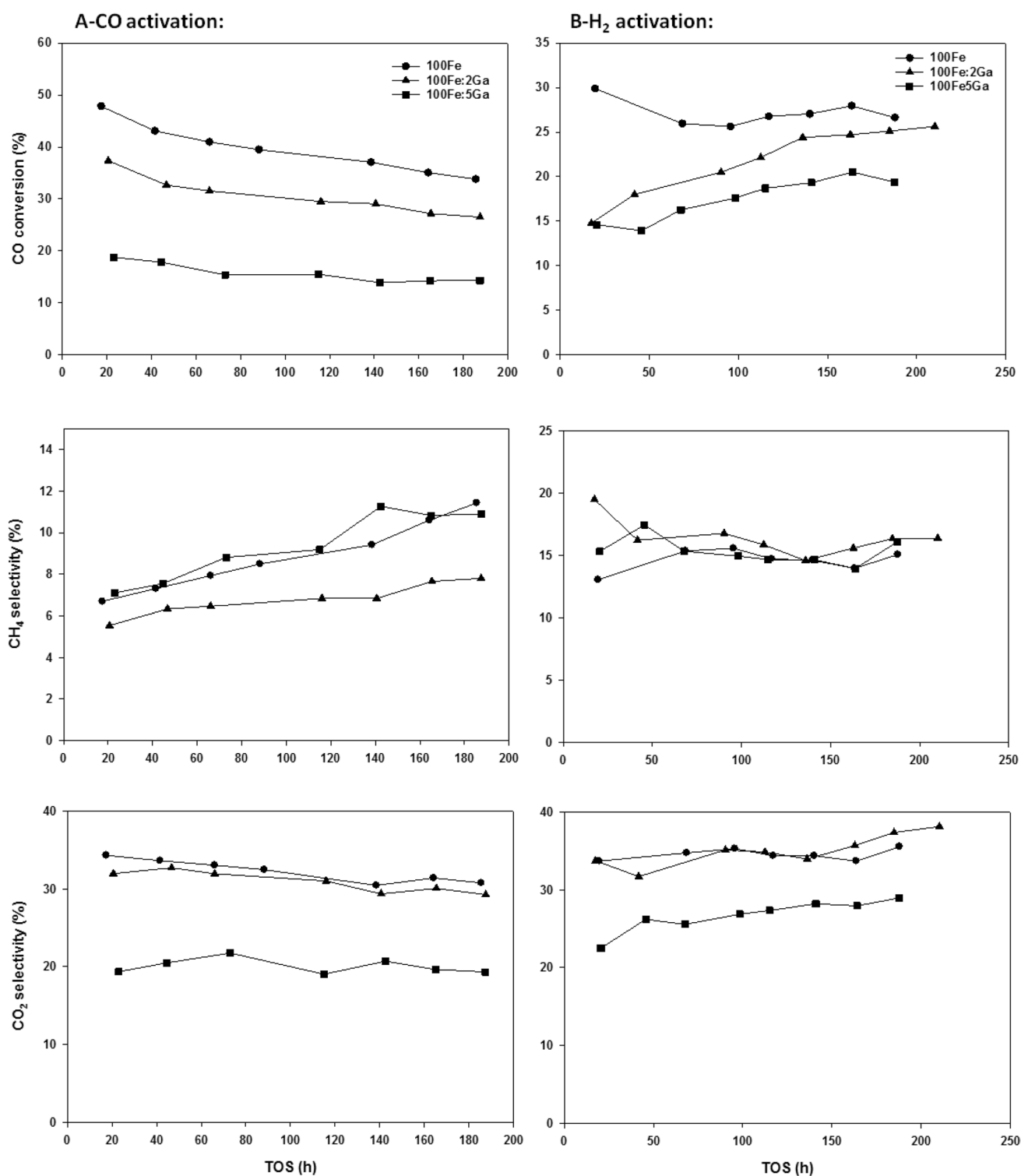**Fig. 5** Temperature programmed decarburization profiles for iron samples after CO activation

Fig. 6 Effect of activation methods (**a** CO activation, **b** H$_2$ activation) on FT activity and methane and CO$_2$ selectivity of iron catalysts. Reaction conditions: temperature = 270 °C, pressure = 175 PSIG, H$_2$/CO = 1.0, SV = 3.0 slph/g iron oxide

for CO$_2$ selectivity. The addition of gallium dropped CO$_2$ selectivity, as indicated by the 100Fe:2Ga and 100Fe:5Ga catalysts. 100Fe:2Ga shows 32% CO$_2$ selectivity and

100Fe:5Ga is around 19%, while 100Fe is at 35%. The H$_2$ reduced iron catalyst samples all exhibit a steady trend for CO$_2$ selectivity. Both 100Fe and 100Fe:2Ga shown 35%
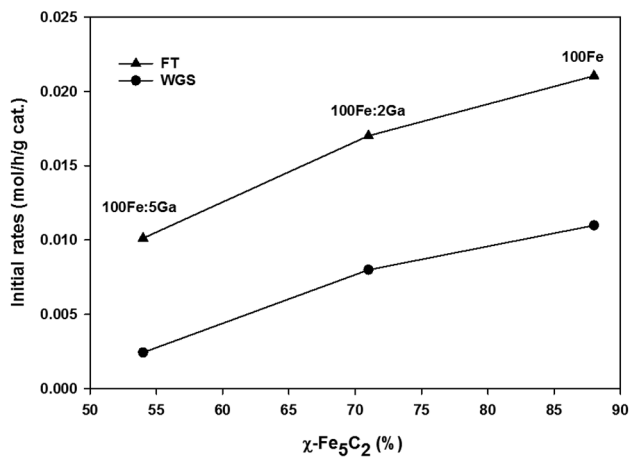
Fig. 7 Correlation between the initial conversion rates (after ~20 h TOS) and the percent χ-Fe_5C_2 present on freshly CO activated iron catalysts. Reaction conditions: temperature = 270 °C, pressure = 175 PSIG, H_2/CO = 1.0, SV = 3.0 slph/g iron oxide

Table 4 The FT activity and product selectivity comparisons between Al_2O_3 and Ga_2O_3 incorporated iron catalysts

Catalysts	100Fe[a]	100Fe:5Ga[a]	100Fe[b]	100Fe:30Al[b]
TOS (h)	88.2	73	97	96
Conversion (%)				
CO	39.5	15.3	75.3	19
H_2	43	19.6	71.9	34.9
H_2+CO	41.3	17.5	73.9	25.3
Hydrocarbon selectivities (%)[c]				
CH_4	9.7	10	8.1	11.1
C_2–C_4	30.8	36.6	10.8	14.7
C_5[b]	59.5	53.4	81.1	74.2

[a]Present work over iron catalysts after CO activation. Reaction conditions: 270 °C, 175 PSIG, H_2/CO = 1.0 and SV = 3.0 nl/h/g catalyst
[b]Wan et al. [20]. Reaction conditions: 260 °C, 200 PSIG, H_2/CO = 0.67 and GHSV = 1000/h
[c]Selectivities are in the weight percent

CO_2 selectivity and 100Fe:5Ga is around 22%. However, this declining trend of CO_2 selectivity with conversion is expected in Fe–FT synthesis.

The active phase of iron for FT synthesis has been a subject of discussion for many years [18–21]. There are many different iron phases (χ-Fe_5C_2, ε-Fe_2C, θ-Fe_3C, metallic Fe, Fe_3O_4 and Fe_2O_3) which can exist simultaneously under the real working condition and they often change with time. Among the iron phases, ε-Fe_2C is claimed to be highly active for FT synthesis [22]. However, the stability of this iron phase under a typical FT synthesis condition is questionable. Many have agreed that χ-Fe_5C_2 is the most active and a highly abundant form of iron during FTS. In this regard, the percent composition of χ-Fe_5C_2 in a fresh activated catalyst was compared with the initial conversion rates for FT and WGS reactions for various catalysts and are shown in Fig. 7. Both FT and WGS activity increased with increasing percentage of the

χ-Fe_5C_2 phase with the undoped and gallium-doped iron catalysts. This indicates that both FT and WGS activity could take place on a similar active site.

The addition of gallium decreases iron carbides content and consequently increased magnetite. This possibly explains why gallium-doped iron catalysts have shown lower CO conversions than the undoped iron catalyst. The olefin and oxygenate selectivity was relatively higher for 100Fe:2Ga compared to 100Fe activated in CO. Similarly, H_2 activated gallium-doped iron catalysts exhibited (Table 3) slightly higher alcohols selectivity (3.8% for 100Fe:2Ga and 4.3% for 100Fe:5Ga) than undoped iron (3.4%). The results strongly indicate that the amount of structural promoter added relative to iron and the method of activation both play a vital role in determining the activity and product selectivity of iron for FT synthesis.

Table 4 shows the comparison of FT activity and product selectivity for Ga_2O_3 and Al_2O_3 incorporated into iron

Table 3 The FT activity and product selectivity of iron catalysts

Description	CO activated			H_2 activated		
	100Fe	100Fe:2Ga	100Fe:5Ga	100Fe	100Fe:2Ga	100Fe:5Ga
Conversion (%)						
CO	32.9	26.5	24.3	25.6	26.7	27.3
H_2	38.5	30.1	15.8	33.1	30.2	34.6
Selectivity (mol, C%)						
Paraffin	32.9	28.2	44.0	29.5	28.4	30.2
Alcohol	2.3	2.9	3.0	3.4	3.8	4.3
Olefin	22.3	29.5	20.2	28.0	22.7	23.3
CO_2	35.4	32.1	25.5	35.5	37.3	28.9
Unidentified	7.1	7.3	7.3	3.6	7.8	13.3

Reaction conditions: temperature = 270 °C, pressure = 175 PSIG, H_2/CO = 1.0, SV = 3.0 slph/g iron oxide

catalysts. Wan et al. [23] concluded that the addition of Al_2O_3 suppresses the reduction of FeO to Fe and further retards the carburization of the iron catalyst. From Table 4, it clearly indicates that the addition of gallium to iron oxide behave in a very similar manner as that of the alumina incorporated iron, i.e., increased light hydrocarbons and decreases C_5^+ formation.

4 Conclusion

The additions of gallium increases the BET surface area but decreases the average pore size of iron oxide. The H_2-TPR data show that gallium did not interfere with the reduction of Fe_2O_3 to Fe_3O_4 but affected the reduction of Fe_3O_4 to metallic iron. ^{57}Fe Mössbauer analysis suggests gallium affects the carburization and reduction of iron oxide differently. On the addition of gallium to iron, CO activated catalysts showed a slight decrease in iron carbide formation from 71 to 54% whereas the H_2 activated catalyst showed a drastic change in the formation of metallic iron from 60 to 6%. XRD and temperature programmed decarburization studies both reveal gallium suppressed the formation of iron carbide and metallic iron during different activation conditions by having strong interactions with FeO_x. Both CO and H_2 conversions were decreased by an increase of gallium content in iron catalysts. The H_2-activated gallium containing iron exhibit initially a lower CO conversion than pure iron but the activity kept increasing over time, in particular 100Fe:2Ga. The selectivity to oxygenates was slightly higher for gallium-containing iron catalysts (4.3, C%) than pure iron (3.4, C%). Between the two activation conditions, H_2-activated iron catalysts produce relatively higher oxygenates content than CO activated iron. The selectivity to methane and carbon dioxide for these catalysts depend mostly on the CO conversions. Both FT and WGS activity correlate with the bulk iron carbide and support our earlier claim that common active sites for both reactions.

References

1. Dry ME (2002) Catal Today 71:227
2. Davis BH (2001) Fuel Process Technol 71:157
3. Jahangiri H, Bennett J, Mahjoubi P, Wilson K, Gu S (2014) Catal Sci Technol 4:2210
4. Abello S, Montane D (2011) ChemSusChem 4:1538
5. Shroff MD, Kalakkad DS, Coulter KE, Kohler SD, Harrington MS, Jackson NB, Sault AG, Datye AK (1995) J Catal 156:185
6. Jothimurugesan K, Spivey JJ, Gangwal SK, Goodwin JG (1998) Stud Surf Sci Catal 119:215
7. Pham HN, Datye AK (2000) Catal Today 58:233
8. Bukur DB, Lang X, Mukesh D, Zimmerman WH, Rasynek MP, Li C (1990) Ind Eng Chem Res 29:1588
9. Jin Y, Xu H, Datye AK (2006) Microsc Microanal 12:124
10. Dlamini H, Motjope T, Joorst G, ter Stege G, Mdleleni M (2002) Catal Lett 78:201
11. Sirimanothan N, Hamdeh HH, Zhang Y, Davis BH (2002) Catal Lett 82:181
12. Sarkar A, Jacobs G, Ji Y, Hamdeh HH, Davis BH (2008) Catal Lett 121:1
13. Yen FS, Chen WC, Yang JM, Hong CT (2002) Nano Lett 2(3):245
14. Bukur DB, Ma W, Vazquez VC (2005) Top Catal 32:135
15. Jacobs G, Pendyala VRR, Martinelli M, Shafer WD, Gnanamani MK, Khalid S, MacLennan A, Hu Y, Davis BH (2017) Catal Lett 147:1861
16. Li L, Wei W, Behrens M (2012) Solid State Sci 14(7):971
17. Xu J, Bartholomew CH (2005) J Phys Chem B 109:2392
18. Schultz JF, Hall WK, Seligman B, Anderson RB (1955) J Am Chem Soc 77:213
19. Datye AK, Jin Y, Mansker L, Motjope RT, Dlamini TH, Coville NJ (2000) Stud Surf Sci Catal 130:1139
20. Niemantsverdriet JW, Van der Kraan M, Van Dijk WL (1989) J Phys Chem 84:363
21. Xu K, Sun B, Lin J, Wen W, Pei Y, Yan S (2014) Nat Commun 5:5783
22. de Smit E, Cinquini F, Beale AM, Safonova OV, van Beek W, Sautet P, Weckhuysen BM (2010) J Am Chem Soc 132:14928
23. Wan HJ, Wu BS, Zhang CH, Xiang HW, Li YW, Xu BF, Yi F (2007) Catal Commun 8:1538

Affiliations

Charles Beasley[1] · Muthu Kumaran Gnanamani[1] · Hussein H. Hamdeh[2] · Michela Martinelli[1] · Burtron H. Davis[1]

✉ Burtron H. Davis
  burtron.davis@uky.edu

[1] Center for Applied Energy Research, University of Kentucky, 2540 Research Park Drive, Lexington, KY 40511, USA

[2] Department of Physics, Wichita State University, Wichita, KS 67260, USA